Boltzmann approximation of transport properties in thermal lattice gases

Ronald Blaak[1] and David Dubbeldam[2,*]
[1]*Grupo Interdisciplinar de Sistemas Complicados (GISC), Departamento de Matemáticas, Universidad Carlos III de Madrid, Avenida de la Universidad, 30, E-28911, Leganés, Madrid, Spain*
[2]*Informatics Institute, Faculty of Science, University of Amsterdam, Kruislaan 403, 1098 SJ Amsterdam, The Netherlands*
(Received 6 October 2000; published 24 January 2001)

The transport properties of the Grosfils, Boon, and Lallemand model, a two-dimensional isotropic thermal lattice-gas, are evaluated in the Boltzmann approximation. This includes the (self)-diffusion, for which we have introduced an additional and passive color label to the otherwise identical particles in the system. Independently, those results are confirmed by the use of the decay of the velocity autocorrelation function. The theoretical predictions of the dynamical structure factors and results obtained by simulations show an excellent agreement up to fairly large wave vectors. In the hydrodynamic limit of small wave vectors, the Landau-Placzek formulas form an alternative and satisfactory description.

DOI: 10.1103/PhysRevE.63.021109 PACS number(s): 05.20.Dd, 05.50.+q, 05.60.−k

I. INTRODUCTION

Lattice gas automata (LGA), as introduced by Frisch, Hasslacher, and Pomeau (FHP) [1], are particle-based methods defined at the mesoscopic level and capable of simulating macroscopic fluid behavior. Stripped down to their bare essence they describe particles, with discreet positions and velocities, that behave as hard-spheres and follow a cyclic process of propagation to neighboring lattice sites and local collisions. The collisions typically conserve mass and momentum, and in the case of a thermal model, energy. From a statistical mechanics point of view the LGA provide a means to examine many-body systems with considerable gain in efficiency. The models exhibit exact conservation laws, unconditional stability, a large number of degrees of freedom, intrinsic spontaneous fluctuations, low memory consumption, and the inherent spatial locality of the update rules make it ideal for parallel processing.

Most LGA models are restricted to conservation of mass and momentum only. Obviously this approximation is allowed if one is interested in the behavior of an athermal fluid, or systems where the role of temperature is negligible. But in order to make the connection with true fluid dynamics, temperature should be included, otherwise even a simple thermal gradient, or problems related to heat-conduction and Rayleigh-Bernard instability, cannot be simulated. Hence, the additional conservation of energy needs to be incorporated in the collisions in order to obtain a thermal LGA. An additional benefit is that the equilibrium transport properties are dependent on both density and temperature, which provides some extra freedom in tuning them with respect to each other without the necessity to change the collision rules.

A thermal LGA model requires the notion of different energy levels. This can be done by allowing the particles in the LGA to move with different speeds (or allowing the particles to have different masses). A requirement for heat-conduction, in addition to heat-diffusion, is that the model should allow population-mixing, i.e., the number of particles in an energy level is not fixed but can change upon collision. This requires at least three different energy levels. The 19-bits GBL model [2], proposed by Grosfils, Boon, and Lallemand (GBL), is such a model. It is a two-dimensional model formulated on a triangular lattice with hexagonal symmetry, is macroscopically isotropic, and has no spurious invariants. This makes it a suitable candidate to study thermal phenomena. Detailed studies have shown that the GBL model exhibits spontaneous fluctuations in equilibrium as produced in a real thermal fluid [2–4].

In the Boltzmann approximation one neglects correlations between the particles. This assumption results in a solvable set of equations, which enables us to obtain the transport properties. Although this approximation can be easily validated for low densities, it is remarkable that even for higher densities, where this assumption is not valid anymore, it still provides acceptable results. Within this approximation one is able obtain the thermal diffusivity, the viscosity, and the sound damping from the linearized collision operator. The (self)-diffusion, however, is a property which cannot be obtained directly, because it requires particles to be distinguishable. For this purpose we have expanded the GBL model to include color, a method used by Hanon and Boon on a FHP model [5]. This color (red/blue) is a passive label on the particles and does not affect the dynamics. This introduces the extra conservations of red and blue particles, and a mutual exclusion such that a channel can be occupied by either a red or a blue particle, but not both. Hence, a color-blind observer would not be able to distinguish this model from the normal GBL model.

The remainder of this paper is organized as follows. In Sec. II we will give a brief overview of the GBL model and the results of the Boltzmann theory. In Sec. III we expand those ideas by including color in the model. We derive the necessary results for the Landau-Placzek formulas in Sec. IV and compare the theoretical predictions with results obtained by computer simulations. In Sec. V we provide some useful results regarding the symmetries of the linearized collision

*Present address: Department of Chemical Engineering, University of Amsterdam, Nieuwe Achtergracht 166, 1018 WV Amsterdam, The Netherlands; Electronic mail: dubbeldam@its.chem.uva.nl

operator, which we exploit to evaluate the transport coefficients with minimal effort and higher numerical accuracy. We finish in Sec. VI with a brief discussion of our results.

II. BOLTZMANN APPROXIMATION

The GBL model is defined on a triangular lattice with hexagonal symmetry. Particles, residing on the nodes, can be in rest or move with discrete velocities 1, $\sqrt{3}$, or 2 to a (next)-nearest-neighboring node. This results in a maximum of 19 particles per node, because no two particles at the same node are allowed to have the same velocity (exclusion). The state s at a node is characterized by the boolean occupation numbers n_i, where i is the label running over all 19 channels. Maximum collision rules are adopted, such that on collision an output state is randomly selected from all possible states with the same mass, momentum, and energy, including the input state itself. For a more detailed description we refer the reader to Ref. [2].

Due to the boolean nature of LGA, the ensemble average of the occupation numbers in equilibrium, are described by a Fermi-Dirac distribution

$$f_i=\langle n_i\rangle=\frac{1}{1+e^{-\alpha+(1/2)\,\beta c_i^2-\boldsymbol{\gamma}\cdot\boldsymbol{c}_i}}, \tag{1}$$

where α, β, and $\boldsymbol{\gamma}$ are Lagrange multipliers and fixed by setting the value of the average density $\rho=\Sigma_i f_i$, momentum $\rho\boldsymbol{u}=\Sigma_i f_i\boldsymbol{c}_i$, and energy density $\rho e=\frac{1}{2}\Sigma_i f_i c_i^2$. β is the inverse temperature, α/β can be identified with the chemical potential, and γ is a parameter conjugate to the flow velocity. However, we will restrict ourselves to the zero-momentum case by putting $\boldsymbol{\gamma}=0$.

The lattice-gas Boltzmann equation is given by [6,7]

$$f_i(\boldsymbol{r}+\boldsymbol{c}_i,t+1)=f_i(\boldsymbol{r},t)+\Delta_i(f), \tag{2}$$

where the collision term Δ_i is a summation over all pre- and post-collision states s and s'

$$\Delta_i(f)=\sum_{s,s'}P(s)A(s\to s')(s_i'-s_i). \tag{3}$$

The collision operator depends on the transition matrix $A(s\to s')$ and the probability $P(s)$ of occurrence of a state s. The transition matrix is determined by the choice of the collision rules and can easily be obtained. The probability $P(s)$, however, is in general a complicated function due to correlations. For low densities, however, we can adopt the molecular chaos assumption and approximate the particles to be independent and not to exhibit any correlations. It follows immediately that the probability $P(s)$ in equilibrium can be written as

$$P(s)=\prod_i f_i^{s_i}(1-f_i)^{1-s_i}. \tag{4}$$

It is hard to prove whether or not the Boltzmann approximation is valid. Comparison with simulation has shown an excellent agreement at low/intermediate densities, and a reasonably good agreement at high densities. At high densities the collisions are correlated, due to ring collisions. Successful theories has been developed to correct for such correlations, even for models violating detailed-balance [8,9].

Fluctuation theory plays a crucial role in the analysis of microscopic models. Many techniques probe the dynamics of a system by introducing an externally induced field. An alternative route is taken by the Green-Kubo relations, where transport phenomena are expressed as time integrals of autocorrelations functions. According to Onsager, the disturbances created by a weak external perturbation decay in the same way as spontaneous fluctuations in equilibrium. We assume that the perturbations induced by intrinsic, spontaneous fluctuations in the velocity field, are sufficiently weak to justify a first order perturbation analysis [4]. Therefore, we can make a Taylor expansion of the collision term in the neighborhood of the equilibrium distribution (1). Only the first order term in this expansion is required to evaluate the transport coefficients, yielding the linearized collision operator

$$\Omega_{ij}=\frac{\partial\Delta_i}{\partial f_j}=\frac{1}{\kappa_j}\sum_{s,s'}P(s)A(s\to s')(s_i'-s_i)s_j, \tag{5}$$

where $\kappa_i=(\partial f_i/\partial\alpha)_\beta=f_i(1-f_i)$ is the variance in the occupation number. Since the GBL model obeys detailed balance, it follows directly that $(\Omega\kappa)_{ij}$ is symmetric [7], where we used that κ_{ij} is a diagonal matrix with elements κ_i. By introducing the notion of an equivalence class $\mathcal{C}=(M,\mathbf{P},E)$, i.e., a set of all states having the same mass $M=\Sigma_i s_i$, momentum $\mathbf{P}=\Sigma_i s_i\mathbf{c}_i$, and energy $E=\Sigma_i\frac{1}{2}s_i\mathbf{c}_i^2$, we can cast this in a more suitable form for computational purposes. By noting that all states s in the same class have the same probability of occurrence

$$\forall s\in\mathcal{C}\quad P(s)=P(\mathcal{C})=e^{\alpha M-\beta E+\gamma\cdot\mathbf{P}}\prod_i(1-f_i), \tag{6}$$

the maximum collision rules lead to a constant transition probability $A(\mathcal{C})$

$$\forall s,s'\in\mathcal{C}\quad A(s\to s')=A(\mathcal{C})=\frac{1}{|\mathcal{C}|}, \tag{7}$$

where we used $|\mathcal{C}|$ to denote the number of different states in the class $\mathcal{C}$, and by defining

$$\mathcal{C}_i\equiv\sum_{s\in\mathcal{C}}s_i, \tag{8}$$

$$\mathcal{C}_{ij}\equiv\sum_{s\in\mathcal{C}}s_is_j, \tag{9}$$

we can evaluate the symmetric matrix $\Omega\kappa$ by

$$\Omega\kappa_{ij}=\sum_{\mathcal{C}}P(\mathcal{C})\left(\frac{\mathcal{C}_i\mathcal{C}_j}{|\mathcal{C}|}-\mathcal{C}_{ij}\right). \tag{10}$$

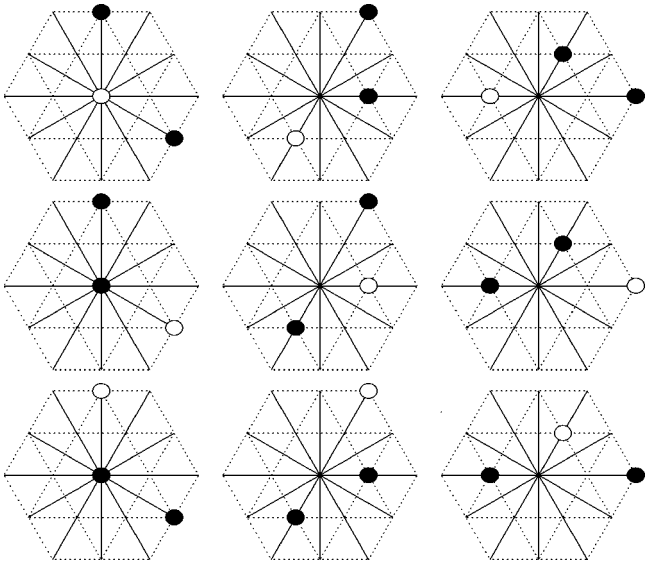

FIG. 1. An example of a equivalence class of size 9: mass 3, momentum $(\frac{3}{2},\frac{1}{2}\sqrt{3})$, energy 3, and 2 red particles. The first row gives already all output states in the GBL model, the second and third row contain only color redistributions.

The benefit of this result is that the double summation over the 2^{19} states is replaced by a single summation over 29 926 different classes. Since we will here only consider the zero-momentum case, we have $\boldsymbol{\gamma}=0$ in Eqs. (1) and (6). Hence, the probability $P(\mathcal{C})$ does not depend on the total momentum, and the classes can be grouped by summing over the label $\boldsymbol{P}$. This results in 280 groups, each contributing a 19 $\times 19$ matrix which can be precomputed, leading to a more efficient evaluation. In fact, a number of classes contain only a single state and will therefore not contribute, such that only 23 388 classes and 248 groups remain.

As a final note we mention that strictly speaking the introduction of $\mathcal{C}_{ij}$ is not necessary, because its summation in Eq. (10) can be evaluated immediately, yielding $\Sigma_{\mathcal{C}}P(\mathcal{C})\mathcal{C}_{ij}=f_i f_j+\kappa_{ij}$. However, it will enable us to make a close connection with the colored version of the GBL model in the next section.

III. COLOR IN GBL

We now introduce a color as a passive label for our particles, i.e., the collisions are not affected by the color of the particles, and we denote the colors by red $(r=1)$ and blue $(b=0)$. For a ''color-blind'' observer this is still the normal GBL model. But apart from randomly selecting a different output state, which conserves mass, momentum, and energy, also the colors need to be randomly reassigned to the particles such that color is conserved as well. An example of such a collision is given in Fig. 1. It is obvious that we can do the collision in two steps, a GBL-like collision followed by a redistribution of the colors over the occupied channels, rather than combining both in a single collision. Note that in this model each channel has three states, it is empty or occupied by either a red or a blue particle, which leads to a total of 3^{19} different states. It is therefore different from a true 38-bits model, because in such a model a red and blue particle can have the same velocity, while in our case this is explicitly excluded.

We now denote by $s=\{s_{i\mu}\}$ the state of a single node, where the first label refers to the velocity channel and the second label to the color. Since we exclude the possibility of two particles with the same speed but different color, we adopt the convention that if only a label for the velocity is used we have used a summation over color, e.g., $s_i=s_{ir}+s_{ib}=s_{i1}+s_{i0}$. In fact, such quantities are the ones which would describe the system for the color-blind observer.

Since color is a passive label for the particles, the average occupation number is given by $f_{i\alpha}=P_\alpha f_i$, where f_i was already defined in Eq. (1) and we introduced the probability of finding a red or blue particle by P_r and $P_b=1-P_r$, respectively. Note that an alternative but equivalent formulation can be obtained by introducing two different chemical potentials in Eq. (1), α_r/β for the red and α_b/β for the blue particles. A simple calculation shows that the connection is made by identifying $e^{\alpha}=e^{\alpha_r}+e^{\alpha_b}$ and $P_\mu=e^{\alpha_\mu}/(e^{\alpha_r}+e^{\alpha_b})$.

Apart from the additional color labels, the expression for the collision operator (3) is unchanged, but the probability $P(s)$ of finding state s is now given by

$$P(s)=\prod_i f_{ir}^{s_{ir}} f_{ib}^{s_{ib}}(1-f_i)^{1-s_i}. \tag{11}$$

Due to the increase in the number of states the transition matrix has to be modified also. Note that a naive generalization of Eq. (4) would lead to $P(s)=\Pi_{i\mu} f_{i\mu}^{s_{i\mu}}(1-f_{i\mu})^{1-s_{i\mu}}$. Such a generalization, however, would not take into account that only a single particle, either red or blue, can exist with a given velocity. This exclusion leads to the above formulation.

In order to proceed we need to clarify the difference between the colored and the uncolored model. In particular the equal-time correlation function of the fluctuations $\delta n_{i\mu}$, which is obtained from the $t=0$ case of the kinetic propagator [3]

$$(\Gamma\kappa)_{i\mu,j\nu}=\langle \delta n_{i\mu}(\boldsymbol{k},t)\,\delta n^*_{j\nu}(\boldsymbol{k},0)\rangle, \tag{12}$$

where * denotes complex conjugation and $\Gamma_{i\mu,j\nu}(\boldsymbol{k},0)=\delta_{i\mu,j\nu}$. In the Boltzmann approximation the different channels are independent and κ is in general found to be a diagonal matrix. Although here fluctuations between particles with different velocities are independent as well, this is not true for the fluctuations δn_{ir} and δn_{ib} with the same velocity but different color. This is a direct consequence of the mutual exclusion of a red and blue particle with the same velocity, in other words the fact that color is a passive label, and hence κ is given by

$$\kappa_{i\mu,j\nu}=\delta_{ij}f_{i\mu}(\delta_{\mu\nu}-f_{i\nu}). \tag{13}$$

Following a similar derivation as for the GBL model [3] the linearized collision operator can be obtained and this results, combined with the matrix κ, in the symmetric matrix

$$(\Omega\kappa)_{i\mu,j\nu}=\frac{\partial\Delta_{i\mu}}{\partial f_{k\sigma}}\kappa_{k\sigma,j\nu}=\sum_{s,s'}P(s)A(s\to s')(s'_{i\mu}-s_{i\mu})s_{j\nu}, \tag{14}$$

where we have adopted the Einstein summation convention. By introducing the colored equivalence classes $\mathcal{C}^*=(M,\boldsymbol{P},E,R)$, with $R=\Sigma_i s_{ir}$ the total number of red particles, we can write this in a form similar to Eq. (10). However, since the collision of particles and the redistribution of colors are independent we can continue a little further. The probability of a state can be written as $P(\mathcal{C}^*)=P_r^R P_b^{M-R}P(\mathcal{C})$, the size of a colored class as $|\mathcal{C}^*|=\binom{M}{R}|\mathcal{C}|$, the summation $\Sigma_{s\in\mathcal{C}^*}s_{i\mu}=\mathcal{C}_i\binom{M-1}{R-\mu}$, and $\Sigma_{s\in\mathcal{C}^*}s_{i\mu}s_{j\nu}=\mathcal{C}_{ij}[\binom{M-1}{R-\mu}\delta_{ij}\delta_{\mu\nu}+\binom{M-2}{R-\mu-\nu}(1-\delta_{ij})]$, where we used the numerical value of the color labels μ and ν in the last expressions. Finally by noticing that $\Sigma_{\mathcal{C}^*}=\Sigma_{\mathcal{C}}\Sigma_{R=0}^{M}$, we find an expression for which the summation over the number of red particles R can be evaluated exact, and after some algebra we obtain

$$\begin{aligned}(\Omega\kappa)_{i\mu,j\nu}=&P_\mu P_\nu\sum_{\mathcal{C}}P(\mathcal{C})\left(\frac{\mathcal{C}_i\mathcal{C}_j}{|\mathcal{C}|}-\mathcal{C}_{ij}\right)\\&+P_\mu(\delta_{\mu\nu}-P_\nu)\sum_{\mathcal{C}}P(\mathcal{C})\left(\frac{\mathcal{C}_i\mathcal{C}_j}{M|\mathcal{C}|}-\delta_{ij}\mathcal{C}_{ij}\right),\end{aligned} \tag{15}$$

where Eq. (10), the uncolored expression $\Omega\kappa_{ij}$, is immediately recognized in the first term.

IV. LANDAU-PLACZEK THEORY

For a detailed derivation of the Landau-Placzek theory of the GBL model we refer the reader to Ref. [3]. Here we will only highlight some of the results and focus on the colored version of the GBL model, which can be derived in an analogous manner and resembles the results of a colored FHP model [5]. However, all expressions for the colored model reduce to expressions for the proper GBL model by summing over all color indices.

In order to proceed we first need to introduce a colored version of the thermal scalar product [7,10]

$$\langle A|B\rangle=\sum_{i\mu j\nu}A(\mathbf{c}_{i\mu})\kappa_{i\mu,j\nu}B(\mathbf{c}_{j\nu}), \tag{16}$$

and adopt the same convention that the matrix κ is attached to the right vector, i.e., $|B\rangle_{i\mu}=\kappa_{i\mu,j\nu}B(\mathbf{c}_{j\nu})$. This colored product was earlier introduced by Hanon and Boon on part of the matrix [5]. The second ingredient which is required are the collisional invariants, which are left eigenvectors of Ω with zero eigenvalue. Four of them, mass, momentum, and energy, already follow directly from the GBL model. In the colored model a fifth invariant emerges due to the fact that the number of red and blue particles are conserved independently. The sum of them giving the mass, which is already taken into account by the GBL model, leaving the fifth invariant to be related to their difference, and we can summarize the invariants by

$$\langle a_n|\Omega=0\quad\Omega|a_n\rangle=0, \tag{17}$$

$$|a_n\rangle=\{|1\rangle,|c_x\rangle,|c_y\rangle,|\tfrac{1}{2}c^2\rangle,|\mathrm{diff}\rangle\}. \tag{18}$$

The invariant $|\mathrm{diff}\rangle$ is a linear combination of the red and blue mass vectors, $|R\rangle$ and $|B\rangle$, and is fixed by constraining it to be orthogonal to the other four invariants. This results in

$$R_{i\mu}=\delta_{\mu r}, \tag{19}$$

$$B_{i\mu}=\delta_{\mu r}, \tag{20}$$

$$|\mathrm{diff}\rangle=\frac{1}{P_r}|R\rangle-\frac{1}{P_b}|B\rangle, \tag{21}$$

and $|\mathrm{diff}\rangle$ becomes the difference between the normalized red and blue densities.

We now proceed by following the method introduced by Résibois and de Leener [11], and consider the single-time step Boltzmann propagator leading to the eigenvalue problem

$$e^{-\imath\mathbf{k}\cdot\mathbf{c}}(\mathbf{1}+\Omega)|\psi(\mathbf{k})\rangle=e^{z(\mathbf{k})}|\psi(\mathbf{k})\rangle, \tag{22}$$

$$\langle\phi(\mathbf{k})|e^{-\imath\mathbf{k}\cdot\mathbf{c}}(\mathbf{1}+\Omega)=e^{z(\mathbf{k})}\langle\phi(\mathbf{k})|, \tag{23}$$

where $e^{-\imath\mathbf{k}\cdot\mathbf{c}}$ has to be interpreted as a 38 dimensional diagonal matrix, and $\mathbf{1}$ is the identity matrix. It can easily be shown from the symmetries of the linearized collision operator (15), that the problem can be split in two independent 19-dimensional problems. The first subproblem is the original problem for GBL with the right eigenvector equation

$$e^{-\imath\mathbf{k}\cdot\mathbf{c}}(\mathbf{1}+\Omega)\kappa\chi(\mathbf{k})=e^{z(\mathbf{k})}\kappa\chi(\mathbf{k}), \tag{24}$$

where the matrices Ω and κ are the normal GBL versions and we explicitly included the later one to compare it with the second subproblem

$$e^{-\imath\mathbf{k}\cdot\mathbf{c}}(\mathbf{1}+\Omega')f\chi'(\mathbf{k})=e^{z'(\mathbf{k})}f\chi'(\mathbf{k}). \tag{25}$$

Here we used that f is a diagonal matrix with elements f_i, and have denoted the color independent, symmetric matrix in the second term of Eq. (15) by $\Omega' f$. The solution of the second subproblem is similar to that of the GBL model, albeit that the thermal scalar product should be modified by using f as a kernel, rather than κ.

The complete set of solutions for the full problem (22) is now obtained by modifying the two sets of solutions for both subproblems with an additional color dependence

$$\psi_{i\mu}(\mathbf{k})=\chi_i(\mathbf{k})\quad\psi_{i\mu}(\mathbf{k})=\left(\frac{\delta_{\mu r}}{P_r}-\frac{\delta_{\mu b}}{P_b}\right)\chi'_i(\mathbf{k}). \tag{26}$$

TABLE I. The eigenvectors, currents, and eigenvalues to dominant order in the limit $\boldsymbol{k}\to 0$.

Viscosity	$\psi_\perp^{(0)}=c_\perp$	$j_\perp=c_{/\!/}c_\perp$	$z_\perp=-\nu k^2$
Thermal diffusivity	$\psi_T^{(0)}=s$	$j_T=c_{/\!/}s$	$z_T=-D_T k^2$
Sound damping	$\psi_\pm^{(0)}=p\pm c_s c_{/\!/}$	$j_\pm=c_{/\!/}s\pm c_s(c_{/\!/}^2-p)$	$z_\pm=-(\pm c_s k+\Gamma k^2)$
(self-)diffusion	$\psi_{\rm diff}^{(0)}=(\text{diff})$	$j_{\rm diff}=c_{/\!/}(\text{diff})$	$z_{\rm diff}=-D_C k^2$

As in the case for the GBL model, the symmetries of the matrices cause the left and right eigenvectors to be related by $\phi_m(\mathbf{k})=e^{\imath \boldsymbol{k}\cdot\boldsymbol{c}}\psi_m(\mathbf{k})/\mathcal{M}_m$, and form a complete biorthonormal set

$$\sum_m |\psi_m\rangle\langle\phi_m| = \mathbf{1} \quad \langle\phi_m|\psi_n\rangle=\delta_{mn}, \tag{27}$$

where we used m and n to label the different eigenfunctions and introduced the normalization constants $\mathcal{M}_m$. Note that the eigenvectors (26) that belong to a different subset are already orthogonal by contracting the color label. From a physical point of view this is of course to be expected, because this will ensure that the two sets cannot couple. If they would, a color-blind observer would have been able to detect a difference between the GBL model and its colored relative.

The next step in the procedure would be to realize that the slow hydrodynamic modes carrying the transport properties have $z(\boldsymbol{k})\to 0$ for small values of $\boldsymbol{k}$. This justifies a Taylor expansion of the eigenvectors and eigenvalues in terms of $|\boldsymbol{k}|$, and we solve the resulting set of equations for successive orders. However, since we have already indicated that the color modes and uncolored modes do not couple, we refer the reader to Ref. [3] for a detailed analysis and have listed the results for the lowest order eigenvector, the current, and up to second order eigenvalues of the GBL model in Table I, including the additional color mode which we have in our model. These results contain the longitudinal and transverse velocity, $c_{/\!/}=\hat{\boldsymbol{k}}\cdot\boldsymbol{c}$ and $c_\perp=\hat{\boldsymbol{k}}_\perp\cdot\boldsymbol{c}$ respectively, the microscopic pressure $p=\frac{1}{2}c^2$, and the entropy $s=p-c_s^2$, where the adiabatic speed of sound c_s is determined such that the microscopic pressure and entropy are orthogonal, i.e., $\langle s|p\rangle=0$. The transport coefficients turn out to be the second order terms in the eigenvalues $z^{(2)}$, which are the viscosity ν, thermal diffusivity D_T, sound damping Γ, and the (self-) diffusion D_C and follow from the second order equations

$$z_a^{(2)}=-\frac{\left\langle j_a\left|\frac{1}{\Omega}+\frac{1}{2}\right|j_a\right\rangle}{\langle\psi_a^{(0)}|\psi_a^{(0)}\rangle}. \tag{28}$$

Although the existence of collisional invariants, and hence zero eigenvalues, prevent us to invert the matrix Ω, the expression is formally correct, because one can show that the currents j belong to the orthogonal complement of the null space of Ω. In addition we mention the fact that although the transport coefficients do depend on the density and energy of the system, none of them depends on the fraction of red and blue particles as follows directly from the two color independent subproblems (24) and (25) and is expected on the basis of physical arguments.

An example of the full wave-vector dependent eigenvalue spectrum is shown in Fig. 2. In the limit $|\boldsymbol{k}|\to 0$ only the five slow modes go to zero (the real part of the two sound damping modes coincide), confirming the absence of any spurious invariants due to the introduction of color. In the hydrodynamic regime of small wavevector we use the expressions found in Table I to obtain the transport coefficients from the eigenvalue spectrum, as is illustrated in Fig. 3. We also indicated the generalized hydrodynamic regime, where the

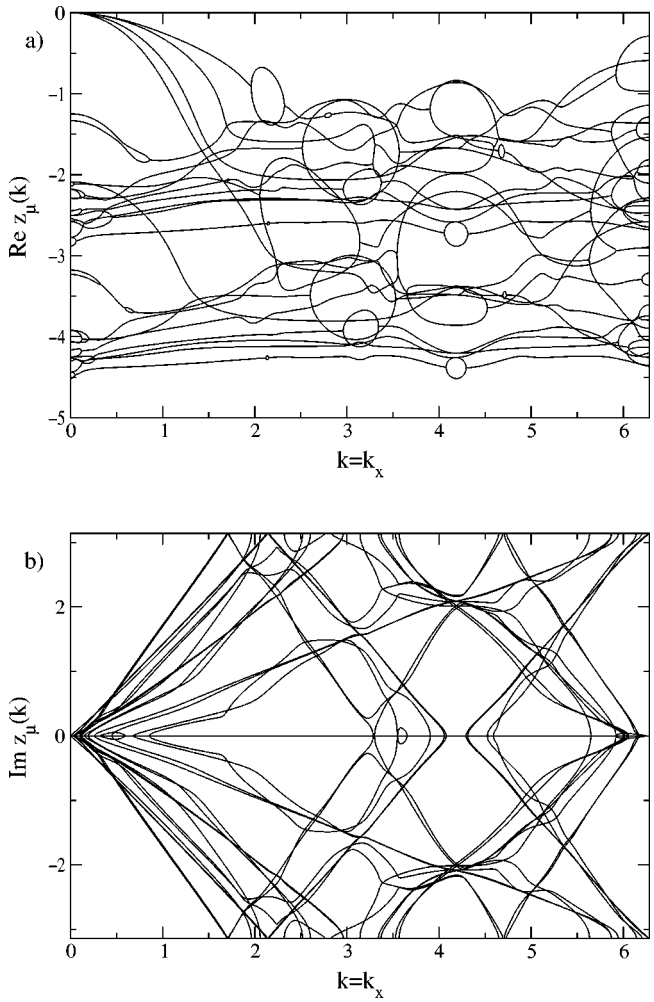

FIG. 2. Full eigenvalue spectrum of the Boltzmann propagator of the colored GBL model as function of the wavevector $|\boldsymbol{k}|$ in reciprocal lattice units. The density and energy density are $\rho=6.0$ and $e=6.7/6.0$, respectively. The spectrum is independent of the fraction of red particles P_r.

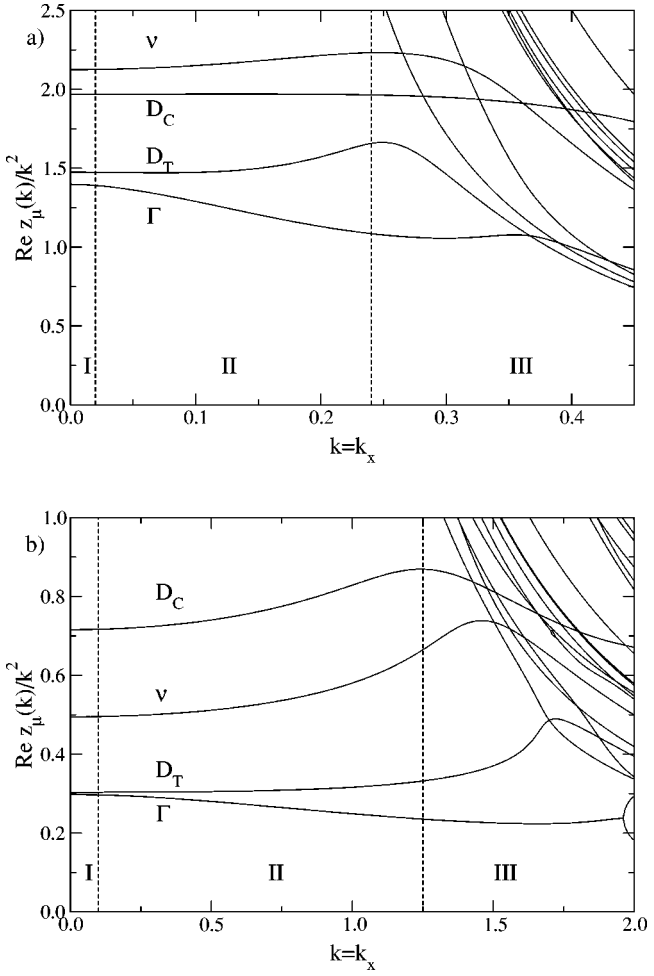

FIG. 3. The wave-vector dependent transport coefficients obtained from the small wave-vector approximation at (a) low density $\rho=1.1$ and $e=1.0$, (b) high density $\rho=6.0$ and $e=6.7/6.0$. The wave vector k is measured in reciprocal lattice units. In the hydrodynamic regime I the transport properties are approximately constant. Regime II characterizes the generalized hydrodynamic regime where the transport properties become strongly k dependent. At still higher k values to regime crosses over into the kinetic regime III, where the kinetic modes become of comparable order as the hydrodynamic modes.

transport properties become strongly k-dependent, and the kinetic regime, where the kinetic modes become of comparable order as the hydrodynamic modes.

It has been shown that the dynamic structure factor

$$\rho S(\boldsymbol{k},\omega)=2\ \mathrm{Re}\langle\rho|(e^{i\omega+\imath\boldsymbol{k}\cdot\boldsymbol{c}}-\mathbf{1}-\Omega)^{-1}+\tfrac{1}{2}|\rho\rangle, \quad (29)$$

in the Boltzmann approximation can be evaluated by [3]

$$\rho S(\boldsymbol{k},\omega)=2\ \mathrm{Re}\sum_m \mathcal{N}_m\mathcal{D}_m, \quad (30)$$

$$\mathcal{N}_m\equiv\langle\rho|\psi_m\rangle\langle\phi_m|\rho\rangle, \quad (31)$$

$$\mathcal{D}_m\equiv\frac{1}{e^{\imath\omega-\imath z_m(\boldsymbol{k})}-1}+\frac{1}{2}, \quad (32)$$

where property (27) has been used to eliminate the matrix Ω, and the expression can be normalized after division by $\rho S(\boldsymbol{k})=\langle\rho|\rho\rangle$. Since the collisional invariant $|\rho\rangle$ is a vector that lies in the GBL part of the model, it is orthogonal to the 19 color modes, which therefore, as expected, do not contribute.

In the colored model we can follow a similar approach to obtain the red mass dynamic structure factor, which is defined as the space and time Fourier transform of the red-red density correlation [5]

$$\langle\delta\rho^{\mathrm{red}}(\boldsymbol{r},t)\,\delta\rho^{\mathrm{red}}(0,0)\rangle, \quad (33)$$

where the red mass density is given by $\rho^{\mathrm{red}}(\boldsymbol{r},t)=\Sigma_i n_{ir}(\boldsymbol{r},t)$. Following the same procedure we obtain the red mass dynamic structure factor

$$\rho^{\mathrm{red}}S^{\mathrm{red}}(\boldsymbol{k},\omega)=2\ \mathrm{Re}\sum_m \mathcal{N}_m^{\mathrm{red}}\mathcal{D}_m, \quad (34)$$

$$\mathcal{N}_m^{\mathrm{red}}\equiv\langle R|\psi_m\rangle\langle\phi_m|R\rangle. \quad (35)$$

But since $|R\rangle$ does not fall completely within either of the two subproblems, we now get a contribution from all 38 modes.

Apart from the five slow hydrodynamic modes related to the transport properties, one also obtain a number of fast kinetic modes. In the hydrodynamic regime of small $\boldsymbol{k}$ and ω these have $\mathrm{Re}\,z_m(0)<0$ and decay exponentially. This is exploited by the Landau-Placzek formula, for which one approximates Eq. (30) by summing only over the slow modes and expanding up to $\mathcal{O}(k^2)$. This also requires the partial knowledge of the eigenvectors up to order $\mathcal{O}(k)$. The shear mode, however, does not contribute due to parity, and only the thermal diffusivity, sound damping, and diffusion modes remain for which we obtain [3]

$$\mathcal{N}_T^{\mathrm{red}}=P_r^2\mathcal{N}_T=P_r^2\langle\rho|\rho\rangle\frac{\gamma-1}{\gamma}+\mathcal{O}(k^2), \quad (36)$$

$$\mathcal{N}_\pm^{\mathrm{red}}=P_r^2\mathcal{N}_\pm=P_r^2\frac{\langle\rho|\rho\rangle}{2\gamma}\left\{1\pm\frac{\imath k}{c_s}[\Gamma+(\gamma-1)D_T]\right\}+\mathcal{O}(k^2), \quad (37)$$

$$\mathcal{N}_{\mathrm{diff}}^{\mathrm{red}}=P_r^2P_b^2\langle\mathrm{diff}|\mathrm{diff}\rangle+\mathcal{O}(k^2), \quad (38)$$

where $\gamma=1+\langle s|s\rangle/\langle p|p\rangle$. By using the normalization $\rho^{\mathrm{red}}S^{\mathrm{red}}(\boldsymbol{k})=\langle R|R\rangle$, we obtain for the Landau-Placzek expression of the red mass dynamic structure factor

$$\frac{S^{\mathrm{red}}(\boldsymbol{k},\omega)}{S^{\mathrm{red}}(\boldsymbol{k})}=\frac{P_r^2\langle\rho|\rho\rangle}{\langle R|R\rangle}\frac{S(\boldsymbol{k},\omega)}{S(\boldsymbol{k})}+\frac{P_r^2P_b^2\langle\mathrm{diff}|\mathrm{diff}\rangle}{\langle R|R\rangle}\frac{2D_Ck^2}{\omega^2+(D_Ck^2)^2}. \quad (39)$$

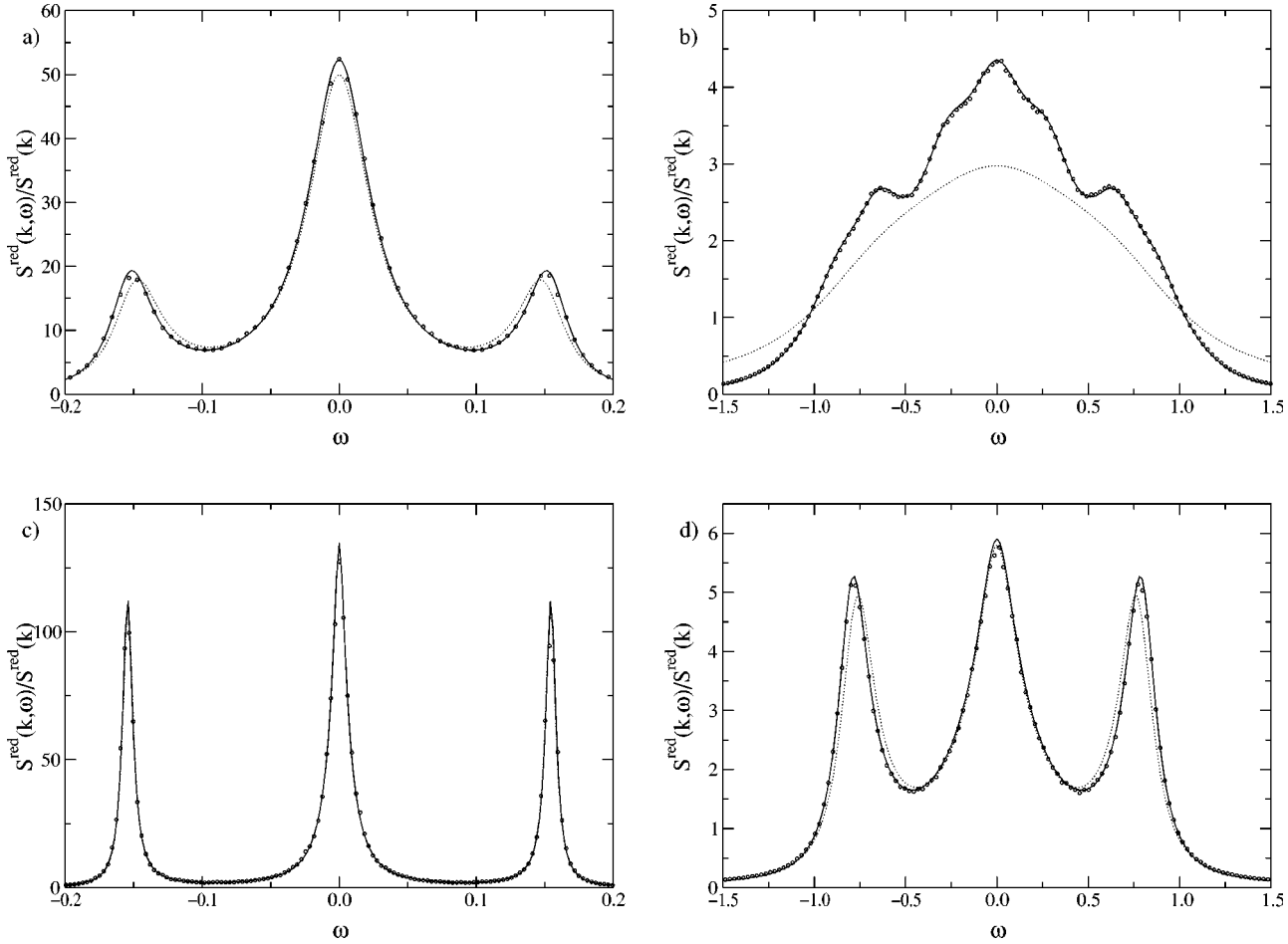

FIG. 4. The red power spectrum at low density $\rho=1.1$, $e=1.0$, $P_r=0.5$ [a, b] and high density $\rho=6.0$, $e=6.7/6.0$, $P_r=0.75$ [c, d]. The wave vectors are $\mathbf{k}_x=5\times 2\pi/256$ [a, c] and $\mathbf{k}_x=25\times 2\pi/256$ [b, d]. The solid line is the Boltzmann prediction (34), the dashed line is the Landau-Placzek approximation (39), and the points are simulation results (gridsize 256×256, time steps 3.5×10^6). The wave vector k is given in reciprocal lattice units, ω in reciprocal time ($2\pi/T$, with T the total number of time steps), and the spectral functions in reciprocal ω units.

This is the normal dynamic structure factor, but with an additional diffusion peak at the same location as the one due to the thermal diffusivity.

In Fig. 4 we show results for the red mass dynamical structure factor for low and higher densities and two different wave vectors. We compare the Boltzmann (34) and Landau-Placzek predictions (39) with simulations performed on a 256×256 grid. As expected for the smaller wave vector the agreement between them is good, but for the larger wave vector the Landau-Placzek curve, specially for the lower density, deviates significantly, while the Boltzmann prediction is still good. This is merely an illustration that we are outside the hydrodynamic regime. As we can see from Fig. 3 we are for the higher density already in the generalized hydrodynamic regime, while for the lower density we even shifted to the kinetic regime.

We also can consider the fluctuations in the difference between the normalized red and blue densities

$$\rho^{\mathrm{diff}}(\boldsymbol{r},t)=\frac{\rho^{\mathrm{red}}(\boldsymbol{r},t)}{P_r}-\frac{\rho^{\mathrm{blue}}(\boldsymbol{r},t)}{P_b}. \tag{40}$$

Following the same route this leads to a dynamical structure factor containing terms of the type $\langle \mathrm{diff}|\psi_m\rangle$. Hence, it will be completely independent of the modes found in the GBL model, and the Landau-Placzek approximation leads to a single Lorentzian

$$\frac{S^{\mathrm{diff}}(\boldsymbol{k},\omega)}{S^{\mathrm{diff}}(\boldsymbol{k})}=\frac{2D_C k^2}{\omega^2+(D_C k^2)^2}. \tag{41}$$

Note that it is not dependent on the fraction of red and blue particles in the system. It also shows that the red mass dynamic structure factor is a simple linear combination of the normal and color difference dynamic structure factors, where only both coefficients depend on the fraction of red and blue particles in the system, a result which also could have been obtained from the identity $|R\rangle=P_r|\rho\rangle+P_rP_b|\mathrm{diff}\rangle$ and the fact that $|\rho\rangle$ and $|\mathrm{diff}\rangle$ are orthogonal.

In Fig. 5 an example of the color difference dynamic structure factor at a density $\rho=10.0$ obtained by simulations is shown and compared with the theoretical curves. From the width of the peak at half-height the diffusion constant is

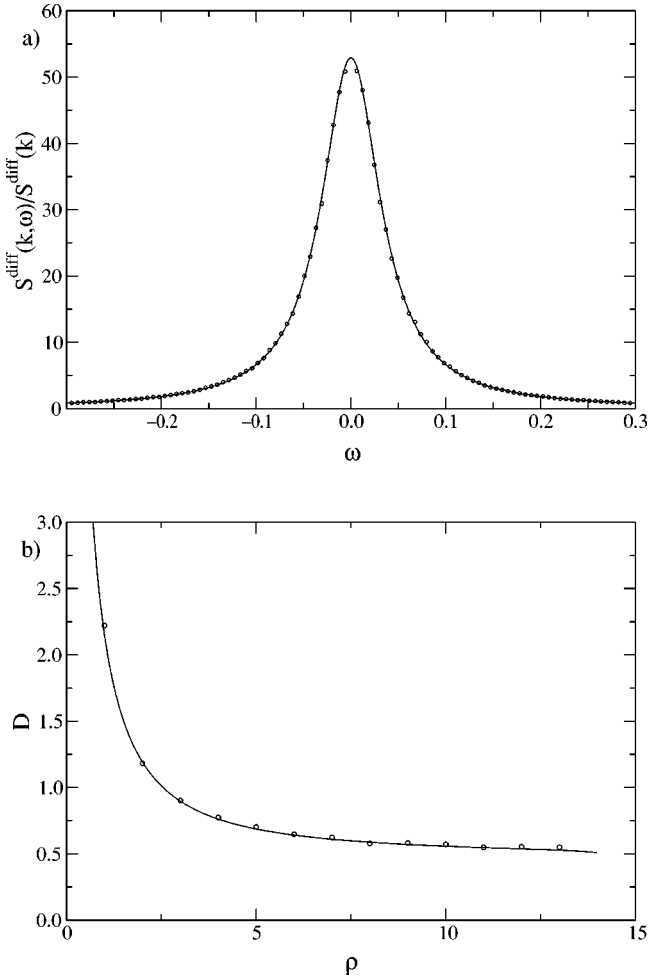

FIG. 5. (a) Dynamic structure factor of the diffusion for density $\rho=10.0$, energy density $e=0.8$, and wave vector $k_x=12\times(2\pi/256)$. (b) (Self)-diffusion as a function of density for fixed energy density $e=1.0$. The points are simulation results, the solid line is the theoretical prediction. The difference between Boltzmann and Landau-Placzek is negligible. Simulations were done on a 256×256 system with $P_r=0.75$ and for time steps 1×10^6.

obtained. The simulations show an excellent agreement with theory. Simulations at very high density $\rho=18.5$ gave no evidence for the unexpected coupling between the diffusion mode and any of the other hydrodynamic modes as was found for the 14-bit model [5]. As a possible explanation we suggest that the ρ^{diff} which was used depends in a nonlinear way on ρ. This would therefore lead to a nonzero contribution from the normal dynamic structure factor, and explain the location and size of the additional peaks by being small contributions of the Brillouin peaks.

V. TRANSPORT COEFFICIENTS

The transport coefficients can now be obtained in two ways. One can solve the eigenvalue problem (22) numerically for small wave vectors and use the formulas in Table I to obtain the desired results, or, alternatively, use the Green-Kubo relations (28). The two routes are equivalent, and the choice made is a matter of convenience. We will adopt here the second method, because it allows for a more efficient and accurate determination of the quantities of interest. Moreover, we do not have to concern ourselves with the problem, which eigenvalue corresponds to which transport coefficient. In what follows we first will restrict ourselves to the uncolored GBL model, because the transport coefficients are not dependent on the presence of color in the system. This also means that we postpone the discussion of the diffusion to a later point.

A. Symmetries of the collision matrix

The solution of Eq. (28) requires us to find a vector A_a such that $\Omega|A_a\rangle=|j_a\rangle$. This vector is not unique, because one could add an arbitrary linear combination of collisional invariants, which are orthogonal to the currents. As an alternative one can decompose $|j_a\rangle$ in terms of eigenfunctions of the collision matrix Ω defined by

$$\Omega|\psi_n\rangle=\omega_n|\psi_n\rangle, \tag{42}$$

because by using a relation similar to (27) and the relation between left and right eigenfunctions one obtains that a transport coefficient L_a is given by [7]

$$L_a=-\frac{1}{\langle\psi_a^{(0)}|\psi_a^{(0)}\rangle}\sum_n\frac{\langle j_a|\psi_n\rangle|^2}{\langle\psi_n|\psi_n\rangle}\left(\frac{1}{\omega_n}+\frac{1}{2}\right). \tag{43}$$

Note that since the currents are orthogonal to the collisional invariants the eigenvalues appearing in the summation are all nonzero.

For the 4-bits HPP model, 6- and 7-bits FHP models on a triangular lattice, 8- and 9-bits models on a square lattice, and even for the 24-bits FCHC model, it turns out that $|j_a\rangle$ itself is an eigenfunction of Ω (see Ref. [7] and references therein). In general, however, this is not the case and the current is a combination of a number of eigenfunctions. In order to understand which and how many eigenfunctions are coupled to a given transport property a more detailed analysis of the matrix Ω is required.

Although the matrix Ω_{ij} itself is not symmetric in its labels, it obeys a number of other symmetries. Their origin is simply due to the symmetry of the lattice on which it is defined. In the case of a triangular lattice with hexagonal symmetry and in the absence of a symmetry breaking feature, such as an overall nonzero flow, the system should be invariant under any of the 12 transformations of the group T mapping a node on itself. These transformations are formed from the combinations of the rotation R over an angle $\pi/3$ and its multiples, and the reflection S_x in the x axis.

If we now let Ω act on an arbitrary vector $\Sigma_n\alpha_n\phi^{(n)}$, where the $\phi_i^{(n)}$ form a complete set of basis vectors, we obtain

$$\Omega_{ij}\sum_n\ \alpha_n\phi_j^{(n)}=\sum_n\ \beta_n\phi_i^{(n)}, \tag{44}$$

where the α_n and β_n are some numerical coefficients. If G is a proper subgroup of the group T of all transformations that

map a node on itself, and take the sum over all elements $g \in G$ acting on the above equations we get

$$\Omega \sum_n \alpha_n \chi^{(n)} = \sum_n \beta_n \chi^{(n)}, \tag{45}$$

where we have introduced a set of symmetry adapted vectors $\chi^{(n)}$ corresponding to the group G by

$$\chi^{(n)} = \frac{1}{|G|} \sum_{g \in G} g(\phi_i^{(n)}), \tag{46}$$

and used that $t(\Omega) = \Omega$ for all $t \in T$. Since in general $g(\phi_i^{(n)}) \neq \phi_i^{(n)}$ and using some general properties of group theory it can easily be seen that some of these vectors will be identical. Therefore the number of χ's will be less than the number of ϕ's and will span an invariant subspace of Ω. If the group G would be either the identity or a noncomplete subgroup of the transformations in T their numbers could also be the same.

It is important to observe that the transformations $t \in T$ only transform channels into channels belonging to the same ''ring,'' where a ring is formed by all channels which can be obtained by applying all transformations in T on a specific channel. In the GBL model such a ring would contain all six channels corresponding to the same absolute velocity. Only the velocity zero would lead to a ring of one channel. If an extension would be made by including higher velocities, e.g., a 31-bits model, also rings with 12 channels exist. Because of the hexagonal lattice symmetry a ring can contain only one, six, or twelve channels.

The fluctuations inside a single ring of 12 channels could of course be written in terms of the 12 independent vectors $\cos(n\theta)$ and $\sin(n\theta)$, where $n=0,\ldots,5$ and $n=1,\ldots,6$ respectively, and θ is the angle made by the direction of the velocity with respect to the positive x axis. Using these as our basis vectors $\phi^{(n)}$, and the three groups $\{\mathbf{1}, S_x\}$, $\{\mathbf{1}, R^3\}$, and $\{\mathbf{1}, R^2, R^4\}$ as the subgroups we find that Ω gives rise to at most eight different invariant subspaces. Four of them being one-dimensional are described by the symmetries 1, $\cos(3\theta)$, $\sin(3\theta)$, and $\sin(6\theta)$, and the other four all being two-dimensional and described by the sets $\{\cos(\theta),\cos(5\theta)\}$, $\{\sin(\theta),\sin(5\theta)\}$, $\{\cos(2\theta),\cos(4\theta)\}$, and $\{\sin(2\theta),\sin(4\theta)\}$. The different subspaces are automatically orthogonal. The two vectors spanning a two-dimensional subspace, however, are only independent with respect to each other, but one can easily construct an orthogonal basis. Although we started with the sine and cosine functions, this is not necessary, because the correct forms are automatically obtained from the full analysis.

The extension made to include the different rings is straightforward after realizing that a set of vectors can be made to correspond to each $\cos(n\theta)$ or $\sin(n\theta)$ by defining a ϕ for each ring as described above and to be zero elsewhere. In this way a simple complete and orthogonal basis is constructed, which decomposes Ω in invariant subspaces. In the degenerate case that a ring contains only six channels some of the vectors become identical or vanish. Of the eight subspaces only six remain corresponding to 1, $\sin(\theta)$, $\cos(\theta)$, $\sin(2\theta)$, and $\cos(2\theta)$. The last subspace depends on the orientation of the ring and is either $\cos(3\theta)$ or $\sin(3\theta)$. For the zero-velocity channel only the subspace corresponding to 1 remains. Since in the GBL model the ring corresponding to velocity $\sqrt{3}$ is rotated 30 degrees with respect to the rings of velocity 1 and 2, seven different subspaces are found related to the symmetries

$$1 \quad c_x \quad c_y \quad c_x c_y \quad c_x^2 - c_y^2 \quad c_x(c_x^2 - 3c_y^2) \quad c_y(c_y^2 - 3c_x^2). \tag{47}$$

The dimension of the first subspace is four, the next four subspaces are of dimension three and the last two of dimension two and one respectively, which follows from a simple counting of contributions of different rings.

The arguments and reasoning presented here are generally true and applicable to any lattice gas, although the outcome will of course depend on the underlying symmetry of the system under consideration. The matrix κ multiplies the different channels in a ring with the same factor and therefore will have the same invariant subspaces, which, of course, is also valid for $\Omega\kappa$.

B. Temperature and Transport

The transport properties of the GBL model vary with temperature. Temperature, however, is not well-defined in a thermal lattice gas [12]. On the one hand we have the temperature as defined for a Fermion-gas $k_B T = 1/\beta$ [7], on the other hand we could define a kinetic temperature $kT = e$ [13] by assuming a local version of the equipartition theorem, which states that the mean kinetic energy per particle is proportional to the temperature. The constant $k = \lambda^2/2\tau^2$ acts like the Boltzmann constant but depends on distance between neighboring lattice nodes λ and the time step τ. The temperature according to $1/\beta$ leads to the possibility of negative temperatures at higher densities, while the kinetic temperature remains positive. The origin of the difference of the temperature scales lies in the fact that a Fermion-gas is used to model a normal gas. We therefore cannot expect the model to behave as an ideal gas except in the low-density limit.

Another important restriction is the limited set of combinations of densities ρ and energy densities e that can be simulated. The space to which they are confined is shown in Fig. 6. Since we will show the transport coefficients for constant reduced temperature $\theta = e^{\beta/2}$, a few of those lines are included. Note that the case $\theta = 1$ with a constant energy density e corresponds to an athermal model.

For the current related to the shear viscosity we obtained $j_\perp = c_{/} c_\perp = c_x c_y$, where we have chosen the wave vector to be along the x axis of the system. It is now obvious from our discussion in the previous subsection that it lies in a three-dimensional subspace, and hence at most three eigenfunctions of Ω are required in Eq. (43) to obtain the viscosity of which the results are shown in Fig. 7. Moreover, by using an appropriate basis transformation based on those considerations, we do not even have to evaluate the full matrix Ω, but only a 3×3 matrix. This results in a faster evaluation,

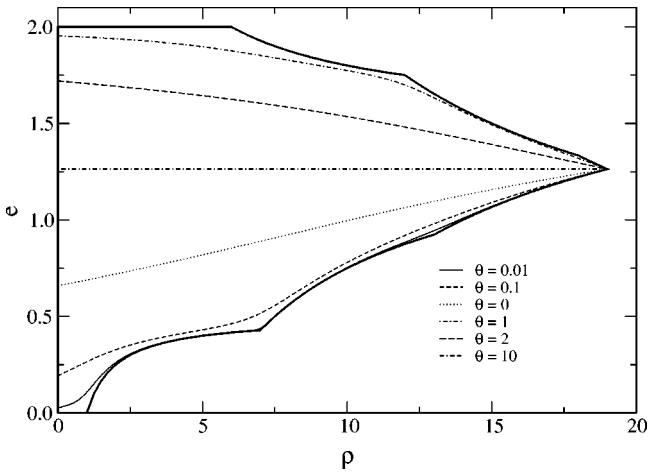

FIG. 6. The space to which the density ρ and energy density e are confined is given by the solid boundaries. Some constant θ lines are included, with the special case $\theta=1$ corresponding to the athermal model.

better numerical accuracy, and, in principle, it even enables us to obtain an analytic formula for the viscosity, although the expression would be rather lengthy.

Only in the limit $\theta\rightarrow 0$ do the transport coefficients show divergencies at the densities $\rho=1$, 7, 13, and 19. This is a direct consequence of the fact that in this zero temperature limit the transition probability of particle exchange between different energy levels goes to zero. At these specific densities each ring of particles is either completely filled or completely empty and hence a static state is reached without any transport. Something similar is observed for the limit $\theta\rightarrow\infty$, although these divergencies are found at $\rho=0$, 6, 12, and 18. The viscosity curves for constant energy density are truncated at a density $\rho<19$, which is simply due to the fact that for the given energy density no higher density can be obtained in the GBL model (Fig. 6).

The current $j_T=c_{\not s}=c_x(\frac{1}{2}c^2-c_s^2)$ also lies in a three-dimensional subspace. But in this case the subspace also contains the collisional invariant c_x and therefore only the two remaining eigenfunctions will contribute to the thermal diffusivity D_T, which is shown in Fig. 8. Note that the curve with $e=1.5$ goes to zero at its highest density, which is not a numerical artifact. The currents of both sound damping modes can be expressed as a linear combination of five eigenfunctions of Ω, but one can obtain the sound damping also immediately from the identity $\Gamma_{\pm}=\frac{1}{2}(\gamma-1)D_T+\frac{1}{2}\nu$.

The zero temperature limit $\theta=0$ represents the ground-state of the model. This means that only in one of the rings particles are able to move. All channels on every node with slower particles are completely filled, while those for faster particles are completely empty. This immediately implies that no energy exchange is possible, and hence the model becomes similar to one or several independent FHP-I models with maximum collision rules. Moreover, since energy has lost its significance, also the thermal diffusivity will disappear. The temperature limit $\theta=\infty$ can be described in the same way, albeit that the rings are filled in the opposite order, or alternatively, as the zero temperature limit of the dual model of holes.

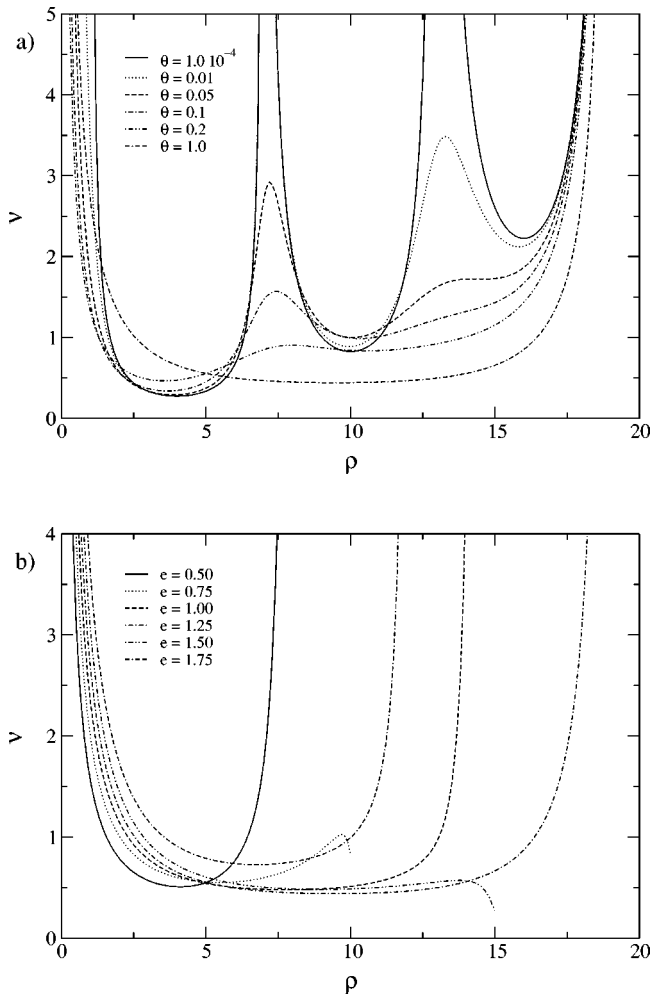

FIG. 7. Shear viscosity as function of the density ρ for various values of (a) the reduced temperature θ and (b) the energy density e.

As a consequence the viscosity in both limits will correspond exactly to the ones obtained from the proper FHP models and is almost identical to the curve $\theta=10^{-4}$ in Fig. 7. The thermal diffusivity, however, is not contained in a FHP model, hence the limit $\theta\rightarrow 0$ and the case $\theta=0$ are truly different. This is illustrated by the fact that for $\rho>7$ the limit is almost identical to the one for $\theta=10^{-4}$ (Fig. 8) for which the thermal diffusivity remains finite, and only in the range $0<\rho<7$ will it go to zero as suggested by that curve.

C. (Self-) Diffusion

In order to obtain the diffusion we could use a similar analysis as in the previous section on the complete colored matrix Ω. But, as we have already seen the current of the diffusion is perpendicular to all GBL modes, and is contained in the matrix Ω' in Eq. (25). So we can restrict ourselves to doing the analysis on this matrix only, where we also need to replace the diagonal matrix κ by that of f.

Also in this case the a decomposition into subspaces can be made, which is obviously the same, and one finds three

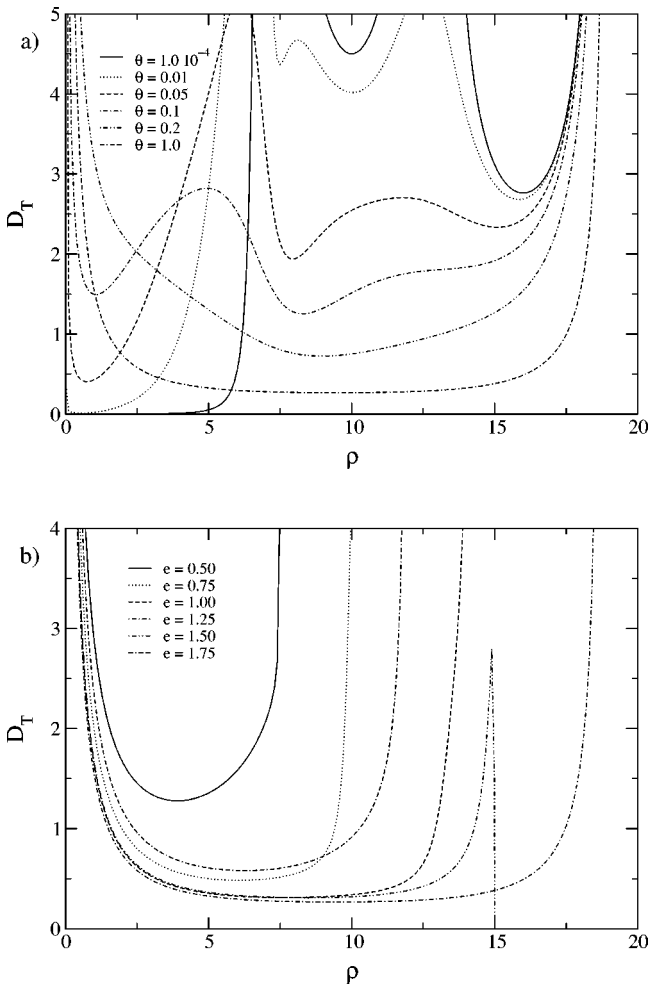

FIG. 8. Thermal diffusivity as function of the density ρ for various values of (a) the reduced temperature θ and (b) the energy density e.

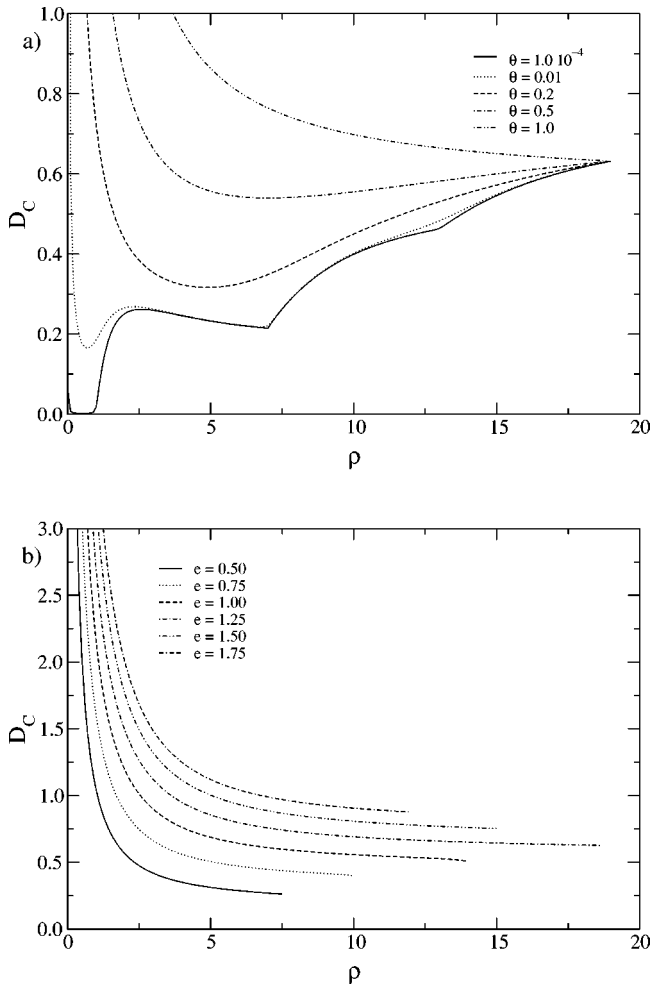

FIG. 9. Self-diffusion as function of the density ρ for various values of (a) the reduced temperature θ and (b) the energy density e.

contributing eigenfunctions to the diffusion shown in Fig. 9. In contrast with the other transport coefficients, no divergencies are found in the zero temperature limit due to the complete filling of rings. A fact that easily can be understood, because even if a ring is completely filled, a redistribution of colors is always possible, provided that the probability of having two colors at a node is nonzero.

The diffusion coefficient can also be obtained from simulations by using the momentum-propagation method [14] and is based on the decay of the velocity autocorrelation function, which turns out to be algebraic. However, in the Boltzmann expression of neglecting correlations it leads to

$$D=\langle v_x^2(0)\rangle\left(\frac{1}{1-Z(1)}-\frac{1}{2}\right), \tag{48}$$

where $Z(1)$ is the normalized velocity autocorrelation function for a single time-step

$$Z(1)=\frac{\langle v_x(0)v_x(1)\rangle}{\langle v_x^2(0)\rangle}. \tag{49}$$

The angular brackets are here referring to an ensemble average and $Z(1)$ can be evaluated by

$$\langle v_x(0)v_x(1)\rangle=\frac{1}{\rho}\sum_s P(s)m(s)u_x^2(s), \tag{50}$$

where $m(s)$ and $u_x(s)$ are the mass and average speed in the x direction of a state. With some algebra it can be shown that the summation can be related to the colored linearized collision operator, the vector $|\mathrm{diff}\rangle$, and its corresponding current. This results in the following expression for the diffusion

$$D=-\frac{\langle j_{\mathrm{diff}}|j_{\mathrm{diff}}\rangle}{\langle \mathrm{diff}|\mathrm{diff}\rangle}\left(\frac{\langle j_{\mathrm{diff}}|j_{\mathrm{diff}}\rangle}{\langle j_{\mathrm{diff}}|\Omega|j_{\mathrm{diff}}\rangle}+\frac{1}{2}\right), \tag{51}$$

and comparison with Eq. (28) shows that this result would have been the true Boltzmann diffusion if the current had been an eigenfunction of Ω, as for instance in an FHP model. As mentioned before, however, the current is composed of three eigenfunctions. Nevertheless, this estimate could be used as a first approximation to the Boltzmann

value and is usually correct within a few percent [7], which explains why the difference between the value for the diffusion obtained by this method and the one obtained from Eq. (43) is negligible.

VI. DISCUSSION

In order to calculate transport coefficients in the Boltzmann approximation, we developed a generally applicable scheme which allows for a fast and in principle analytical evaluation in the case of no-flow. At the cost of some efficiency it could also be extended to include a drift velocity. We use the scheme to evaluate the viscosity, thermal diffusivity, and sound damping in the two dimensional GBL model, but it can easily be extended to other models and higher dimensions. In order to evaluate the (self-) diffusion, we extended the model by attaching a passive color label to the particles and confirmed those results by the use of the Boltzmann approximation of the decay of the velocity autocorrelation function. Some artificial behavior, as divergencies in the transport properties is observed, but can be completely understood.

A comparison of the dynamical structure factors in the colored and uncolored model obtained from simulations with the theoretical curves, show an excellent agreement. In the hydrodynamic regime the agreement between the Boltzmann expression and the Landau-Placzek formula is good.

A final note is made about the confirmation of transport coefficients in simulation. It is virtually impossible to accurately measure a transport coefficient from a lattice-gas simulation for a specific combination of density and temperature. A Poiseuille viscometer fits a parabolic profile to the simulation momentum-density profile. Since the transport coefficients are velocity dependent, due to the lack of Galilean-invariance of LGA models, several measurement with decreasing velocities should be undertaken, where the zero-velocity transport value could be extrapolated by fitting the data with a curve. However, the density and temperature across the channel vary strongly. Another possibility is to measure the transport coefficient from the dynamic structure factor obtained from a simulation. The width of the channel and the wave vector should be chosen in the hydrodynamic area, i.e., the wave vector times the mean-free path should be much smaller than unity. The amount of simulation required to accurately extract the transport coefficients is huge. Therefore, the Boltzmann approximation provides a cheap alternative, which turns out to be accurate enough for many practical purposes, even at high densities.

ACKNOWLEDGMENT

Part of this work was initiated in the group Section Computational Science of the University of Amsterdam, which we like to thank for their hospitality.

[1] U. Frisch, B. Hasslacher, and Y. Pomeau, Phys. Rev. Lett. **56**, 1505 (1986).
[2] P. Grosfils, J.-P. Boon, and P. Lallemand, Phys. Rev. Lett. **68**, 1077 (1992).
[3] P. Grosfils, J.-P. Boon, R. Brito, and M.H. Ernst, Phys. Rev. E **48**, 2655 (1993).
[4] J.-P. Rivet and J.-P. Boon, *Lattice Gas Hydrodynamics, Cambridge Nonlinear Science Nr. 11* (Cambridge University Press, Cambridge, 2001).
[5] D. Hanon and J.P. Boon, Phys. Rev. E **56**, 6331 (1997).
[6] R. Brito, M.H. Ernst, and T.R. Kirkpatrick, J. Stat. Phys. **62**, 283 (1991).
[7] M.H. Ernst and S.P. Das, J. Stat. Phys. **66**, 465 (1992).
[8] H.J. Bussemaker, M.H. Ernst, and J.W. Dufty, J. Stat. Phys. **78**, 1521 (1995).
[9] H.J. Bussemaker and M.H. Ernst, Phys. Rev. E **53**, 5837 (1996).
[10] S.P. Das and M.H. Ernst, Physica A **187**, 191 (1992).
[11] P. Résibois and M. de Leener, *Classical Kinetic Theory of Fluids* (Wiley, New York, 1977).
[12] C. Cercignani, J. Stat. Phys. **87**, 1097 (1997).
[13] B. Chopard and M. Droz, *Celllular Automata Modeling of Physical Systems* (University Press, Cambridge, 1998).
[14] M.A. van der Hoef and D. Frenkel, Phys. Rev. A **41**, 4277 (1990).